

Probing the origin of the microwave anomalous foreground

N. Ysard, M.A. Miville-Deschênes, and L. Verstraete

Institut d'Astrophysique Spatiale, UMR8617, Université Paris-Sud, F-91405, Orsay, France

Preprint online version: June 24, 2021

ABSTRACT

Context. The Galactic anomalous microwave emission detected between 10 and 90 GHz is a major foreground to CMB fluctuations. Well correlated with dust emission at 100 μm , the anomalous foreground is interstellar but its origin is still debated. Possible carriers for this emission are spinning, small dust grains carrying a permanent electric dipole.

Aims. To probe the origin of the anomalous foreground, we compare microwave data to dust IR emission on an angular scale of 1° , and search for specific signatures predicted by models of spinning dust.

Methods. For the anomalous foreground, we use the 23 GHz all-sky map deduced from WMAP data by Miville-Deschênes and collaborators. The infrared dust emission is traced by IRAS data. Models show that spinning dust emission is little sensitive to the intensity of the radiation field (G_0) for $10 \lesssim \nu \lesssim 30$ GHz, while the mid-IR emission produced by the same small dust grains is proportional to G_0 . To test this behaviour in our comparison, we derive G_0 from the dust temperature maps of Schlegel and collaborators.

Results. From all-sky maps, we show that the anomalous foreground is more strongly correlated with the emission of small grains (at 12 μm) than with that of large grains (at 100 μm). In addition, we show that the former correlation is significantly improved when the 12 μm flux is divided by G_0 , as predicted by current models of spinning dust. The results apply to angular scales greater than 1° . Finally, from a model fit of the anomalous foreground, we deduce physical properties for PAHs that are in good agreement with those deduced from mid-IR spectroscopy.

Key words. anomalous foreground – spinning dust emission – interstellar medium – PAH – galactic foregrounds – WMAP – IRIS

1. Introduction

As part of an effort towards accurate measurements of CMB fluctuations, experiments have motivated a detailed study of the Galactic foregrounds in the GHz-range. Kogut et al. (1996), Leitch et al. (1997), and de Oliveira-Costa et al. (1997) found an unexpected emission excess between 10 and 90 GHz, which is correlated with dust far-IR but not with synchrotron emission. To avoid an inaccurate interpretation, this excess has been referred to as an *anomalous foreground*. Low frequency observations have shown that it has a rising spectrum for $\nu \lesssim 30$ GHz (de Oliveira-Costa et al. 1999; Banday et al. 2003; Finkbeiner et al. 2004; Davies et al. 2006). Both this behaviour and also the flux level of the excess are incompatible with what is known about the usual Galactic components in this spectral range: synchrotron, free-free, and thermal dust emission (de Oliveira-Costa et al. 1999, 2004; Lagache 2003; Finkbeiner et al. 2004; Miville-Deschênes et al. 2008). If the anomalous foreground is caused by spinning, small grains as proposed by Draine & Lazarian (1998, hereafter DL98) it should correlate more strongly with the mid-IR emission of small grains (de Oliveira-Costa et al. 2002) than with the large grain (BG) far-IR emission. Until now, there is only incom-

plete evidence that this is the case, the difficulty being the subtraction of zodiacal light in mid-IR data. From a comparison of WMAP data to HI data, Lagache (2003) showed that the anomalous foreground rises with decreasing column density, in a similar way to the emission of small, transiently heated grains. Towards the dark cloud L1622, Casassus et al. (2006) found a stronger spatial correlation between the CBI 31 GHz and the IRAS 12 and 25 μm bands than with the 60 and 100 μm bands. In addition, models predict that the spinning dust emission is little sensitive to the intensity of the radiation field for $10 \lesssim \nu \lesssim 30$ GHz (DL98, Ali-Haïmoud et al. 2009, Ysard & Verstraete 2009 hereafter YV09). Casassus et al. (2008) tested this result in the ρ Oph molecular cloud: by comparing mid-IR (IRS, 13.3 μm) and 31 GHz (CBI) data, they showed that they are well correlated if the former is corrected for the exciting radiation field. In this paper, we further test the above predictions of spinning dust models by comparing, on a 1 degree scale, enhanced IRAS data (IRIS) and the anomalous all-sky map of Miville-Deschênes et al. (2008, hereafter MD08). We also derive some physical properties of dust and compare them to those deduced from IR spectroscopy.

The paper is organized as follows. Section 2 describes the observational predictions of spinning dust models and how they can be used to probe the origin of the anomalous foreground. Section 3 presents the data sets used to reach this goal. Section

4 shows how the anomalous foreground correlates with dust emission. Section 5 lists some remarkable fields and presents the type of information that we expect to derive from the anomalous foreground study. Finally, Section 6 presents our conclusions.

2. Behaviour of the spinning dust emission

Nanometric-sized grains or Polycyclic Aromatic Hydrocarbons (PAHs) emit mostly in the mid-IR, whereas large grains dominate the FIR emission. The PAH emission is known to scale with the intensity of the radiation field G_0 ¹ (Sellgren et al. 1985). This is also true for the emission of large grains and for $G_0 < 100$. We show in Fig. 1 the behaviour of the spinning dust emission with G_0 in photometric bands predicted by our model (YV09). Models predict that the spinning dust emission near 23 GHz is almost independent of G_0 when $0.01 \leq G_0 \leq 100$ (Ali-Haïmoud et al. 2009, YV09, Fig. 1). This has strong observational consequences. If anomalous foreground is spinning dust emission, we expect there to be a stronger correlation between anomalous foreground at 23 GHz and IR emission divided by G_0 than with IR emission alone. Moreover this correlation should be stronger for 12 μm than 100 μm IRAS bands because the former traces the emission of small grains.

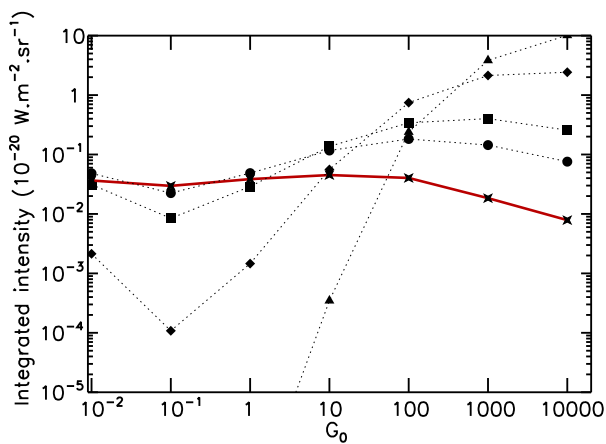


Fig. 1. Results obtained with the model of YV09, for a MRN size distribution ($N_C = 30-216$), where N_C is the number of C-atoms in the PAH and we assume a proton density of $n_H = 30 \text{ cm}^{-3}$. Other gas phase parameters (temperature, and electron, proton, and C^+ abundances) were computed with CLOUDY 05.07 (Ferland et al. 1998) in the optically thin limit and assuming 130 (320) ppm of carbon (oxygen) in the gas phase. Integrated intensity in the WMAP bands vs G_0 : stars (red line) show the 23 GHz band, circles the 33 GHz band, squares the 41 GHz band, diamonds the 61 GHz band, and triangles the 94 GHz band.

¹ Scaling factor for the radiation field integrated between 6 and 13.6 eV. The standard radiation field corresponds to $G_0 = 1$ and to an intensity of $1.6 \times 10^{-3} \text{ erg/s/cm}^2$ (Parravano et al. 2003).

3. Data sets

To carry out these correlations, we need maps of the anomalous and dust emission as well as for the G_0 values. IRAS is a natural data set to study dust IR emission. Our IR template is the new generation of IRAS images, called IRIS (Miville-Deschênes & Lagache 2005), in the 12 and 100 μm bands, which is corrected for most of the remaining instrumental problems of the IRAS/ISSA dataset. Point sources were removed in the IRIS plates (at 5 arcmin resolution) using the method described in Miville-Deschênes & Lagache (2005). The plates were then projected onto the Healpix grid, where an ecliptic-oriented filtering was applied to remove residual zodiacal light emission (Miville-Deschênes et al. in preparation). Finally, the IRIS all-sky maps were convolved with a 1 degree FWHM Gaussian, smoothing out any imperfections related to the point source subtraction.

Miville-Deschênes et al. (2008) performed a separation of components in the WMAP bands, using a physical approach to describe the Galactic foregrounds. We use this anomalous template at 23 GHz, inferred from their “Model 4”. The main assumption made to obtain this map is that polarized emission at 23 GHz is dominated by synchrotron (no assumption about any correlation with dust).

Finally, the G_0 -map is deduced from the BG temperature map of Schlegel et al. (1998) that is inferred from the 140/240 DIRBE ratio. We assume that the interstellar radiation field has the same spectral distribution as the standard field of Mathis et al. (1983), everywhere in the Galaxy, and that the BG spectral index is $\beta = 2$ (Draine & Lee 1984). The energy balance of a single grain of size 0.1 μm then yields $G_0 = (T_{BG}/17.5 \text{ K})^{\beta+4}$. All of these maps have been smoothed to the same angular resolution of 1° .

4. Correlations

Figure 2 shows the all-sky correlation of the 23 GHz anomalous flux with the dust IR emission. The anomalous foreground clearly correlates more strongly with the 12 μm band than the 100 μm (the Pearson correlation factor P is 0.90 and 0.82, respectively). A similar result was obtained by Casassus et al. (2006) towards the LDN 1622 cloud, but here it is the first time that it has been shown to also be true for the entire sky, following the removal of zodiacal light residuals at 12 μm . The correlation is also improved significantly when the dust IR emission is divided by G_0 ($P = 0.90$ to 0.95 , in the case of the 12 μm band²). This improvement concerns $\sim 60\%$ of the sky at 12 μm . These regions are 1.4 to 1.6 times brighter at 23 GHz than the regions for which the division does not improve the correlation. However, in most of the regions where the division by G_0 does not improve the correlation, it also does not make it poorer. It does only for 5% of the sky, which could be explained by the uncertainties in the G_0 values. These correlations show the independence of the anomalous foreground of G_0 at

² Using a Monte Carlo method to simulate thermal noise in the 12 μm map, we find that the Pearson coefficient 0.95 differs significantly from 0.90 with a confidence level greater than 99.9% (using a map containing 786 432 pixels).

23 GHz and its link with the smallest grains. However, since the all-sky correlation is almost as strong with BG emission as with small grains, we are unable to draw firm conclusions at this stage. Across the entire sky, the emissions of PAHs and BGs are known to be correlated well. This is no longer true for particular fields, as we now discuss.

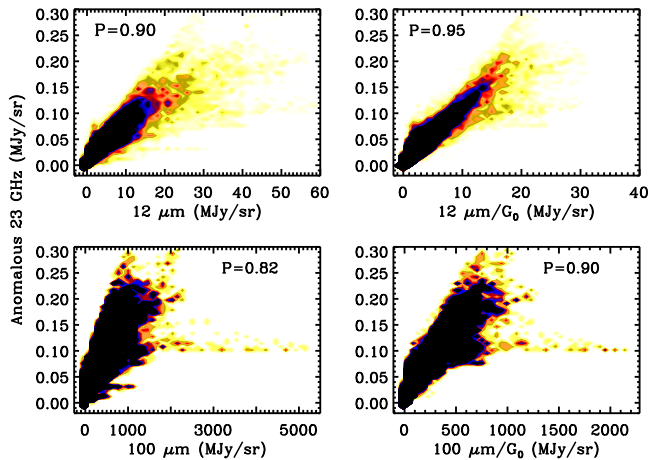


Fig. 2. All-sky correlations. Left panels show the anomalous foreground in the 23 GHz WMAP band versus the dust IR emission in the 12 and 100 μm IRAS bands. In the right panels, the dust IR emission has been divided by G_0 , the intensity of the radiation field. The contrast in point density between yellow and black area is a factor 3. We indicate in each panel the value of the Pearson correlation factor P .

5. Selected fields

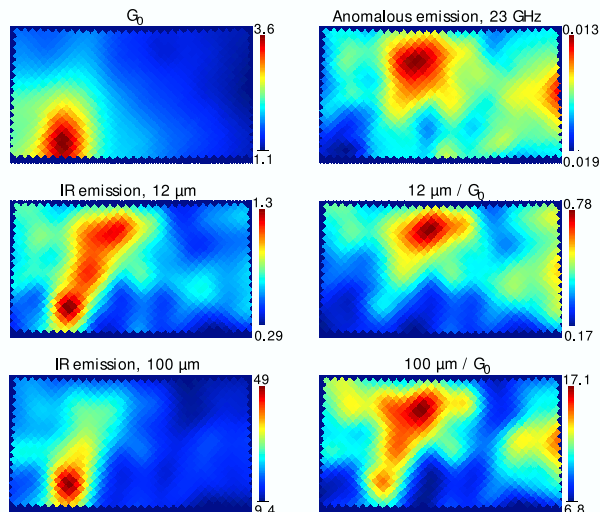


Fig. 3. Field centred on $l = 343.6 \pm 5.25^\circ$ and $b = 22.4 \pm 2.6^\circ$. The 23 GHz, 12 and 100 μm maps are in MJy/sr.

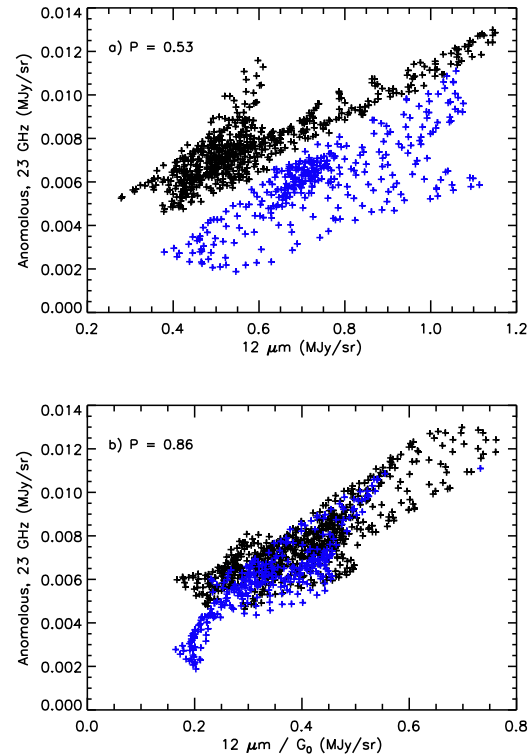


Fig. 4. Field centred on $l = 343.6 \pm 5.25^\circ$ and $b = 22.4 \pm 2.6^\circ$. Correlations between *a*) anomalous foreground at 23 GHz and dust 12 μm emission, and *b*) anomalous foreground at 23 GHz and dust 12 μm emission divided by G_0 . The black crosses show the low- G_0 area (median value equal to 1.4) and the blue ones the high- G_0 area (median equal to 2.3). P is the Pearson's correlation factor.

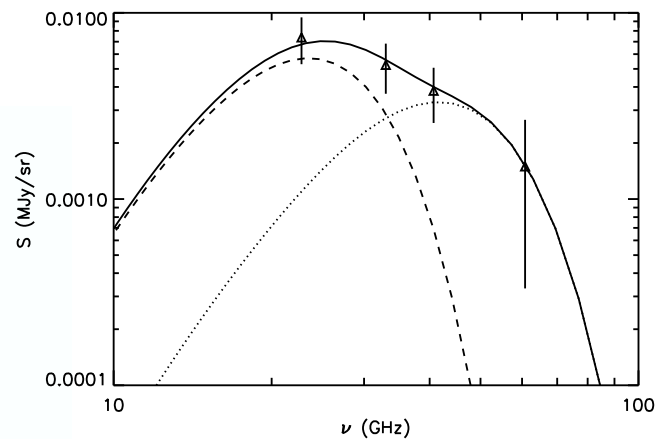


Fig. 5. A representative anomalous spectrum of our selected fields (taken from model 4 of MD08). The solid line is the fit with our model (YV09) comprising contributions from the CNM (10%, dashed line) and from the WNM (90%, dotted line). PAH parameters (see text) are $m = 0.3$ D, and $N_{\text{min}} = 24$ and 48 (CNM and WNM respectively).

To test the spinning dust hypothesis further, we searched for fields of a few squared degrees according to the following cri-

teria: location outside of the Galactic plane, and bright at both 23 GHz and 12 μm with G_0 variations as large as possible. Searching the sky maps by areas of 5° squared, we identified 27 such fields. Figure 3 is an example of one of them. The anomalous and dust brightness maps correlate far more tightly when the latter is divided by G_0^3 . The correlation plots indeed clearly illustrate two cases (Fig. 4a) corresponding to different values of G_0 . The difference disappears when the 12 μm brightness is divided by G_0 (Fig. 4b), as expected if the anomalous foreground is produced by the emission of spinning PAHs.

For 5 of the 27 selected fields, we observe significant spatial variations between the 12 and 100 μm brightness maps (as shown in Fig. 3). In these fields, we note that the correlation between the anomalous foreground and the BG 100 $\mu\text{m}/G_0$ is worse⁴ (Pearson's correlation factor $P = 0.7$ for the field in Fig. 3) than with the smaller grains 12 $\mu\text{m}/G_0$ ($P = 0.86$). This shows that the anomalous foreground is correlated well with BG emission, *only* if BG emission is well correlated with IR emission characteristics of smaller grains. These results are consistent with spinning dust emission.

We further test the spinning hypothesis and attempt to constrain the electric dipole moment of PAHs in the selected fields. As discussed by YV09, the brightness of spinning PAHs at 23 GHz, S_{23} , is given by $N_H S_{PAH} m^2 \epsilon_S$, where N_H is the proton column density, S_{PAH} is the abundance of PAHs, m is a scaling factor inferring the electric dipole moment of PAHs, $\mu(\text{D}) = m \times N^{1/2}$ (where N is the number of atoms in the PAH), and ϵ_S is the rotational luminosity per solid angle and per PAH molecule. The PAH IR brightness in the 12 μm band, I_{12} , is proportional to $N_H S_{PAH} G_0 \epsilon_I$, where ϵ_I is the IR luminosity per solid angle and per PAH. The correlation coefficient between anomalous and IR brightness divided by G_0 is then $m^2 \times \epsilon_S / \epsilon_I$, where ϵ_S depends on the number of carbon atoms in the smallest PAH molecules (N_{min}) and the fractions of neutral cold (CNM) and warm (WNM) diffuse gas. In Fig. 5, we show a representative fit to the observed anomalous foreground with our model. From the 27 selected fields, we find a mean ratio $S_{23}/(I_{12}/G_0) = 1.3 \times 10^{-2}$ with a standard deviation of 4×10^{-3} . Our model fits yield $m = 0.3 - 0.4 \text{ D}$, $N_{min} = 20 - 60$ and about 10% of CNM to account for both the 23 GHz and 12 μm emission. These sizes are currently invoked to explain the 3.3 μm profile in interstellar clouds (Verstraete et al. 2001; Pech et al. 2002) and the m -value is in good agreement with laboratory measurements for organic molecules (DL98). Thus, the rotational and vibrational emission of PAHs, as in current models, can consistently explain the anomalous and 12 μm emission for plausible properties of PAHs.

6. Conclusions

From an all-sky, degree-scale comparison of the 23 GHz anomalous map with dust IR emission, we have found that the

anomalous foreground is well correlated with the 100 μm IRAS band. Using an enhanced set of IRAS maps, we have shown for the first time that the anomalous foreground is correlated with the 12 μm band across the entire sky and that the correlation is tighter than with the 100 μm flux. This correlation becomes even tighter when the 12 μm flux is corrected for the intensity of the radiation field G_0 , indicating that the anomalous emission is independent of G_0 at 23 GHz on a 1 degree scale. These findings strongly argue in favor of a spinning dust origin to the anomalous foreground. Current models predict that the spinning dust emission is dominated by the smallest dust grains (PAHs) carrying the 12 μm flux and that the corresponding 23 GHz emission is almost independent of G_0 . From a model fit of both microwave and IR data in selected fields with strong G_0 contrast, we deduce the physical properties of PAHs (sizes, electric dipole moment) that are in good agreement with results obtained from mid-IR spectroscopy.

Acknowledgements. We thank our referee, Simon Casassus, for his insightful comments that helped in improving the content of this letter. Some of the results in this paper have been derived using the HEALPix package (Górski et al. 2005). This paper used the photoionization code CLOUDY (Ferland et al. 1998).

References

- Banday, A. J., Dickinson, C., Davies, R. D., Davis, R. J., & Górski, K. M. 2003, MNRAS, 345, 897
- Casassus, S., Cabrera, G. F., Förster, F., et al. 2006, ApJ, 639, 951
- Casassus, S., Dickinson, C., Cleary, K., et al. 2008, MNRAS, 391, 1075
- Davies, R. D., Dickinson, C., Banday, A. J., et al. 2006, MNRAS, 370, 1125
- de Oliveira-Costa, A., Kogut, A., Devlin, M. J., et al. 1997, ApJ, 482, L17+
- de Oliveira-Costa, A., Tegmark, M., Davies, R. D., et al. 2004, ApJ, 606, L89
- de Oliveira-Costa, A., Tegmark, M., Finkbeiner, D. P., et al. 2002, ApJ, 567, 363
- de Oliveira-Costa, A., Tegmark, M., Gutierrez, C. M., et al. 1999, ApJ, 527, L9
- Draine, B. T. & Lee, H. M. 1984, ApJ, 285, 89
- Ferland, G. J., Korista, K. T., Verner, D. A., et al. 1998, PASP, 110, 761
- Finkbeiner, D. P., Langston, G. I., & Minter, A. H. 2004, ApJ, 617, 350
- Górski, K. M., Hivon, E., Banday, A. J., et al. 2005, ApJ, 622, 759
- Kogut, A., Banday, A. J., Bennett, C. L., et al. 1996, ApJ, 460, 1
- Lagache, G. 2003, A&A, 405, 813
- Leitch, E. M., Readhead, A. C. S., Pearson, T. J., & Myers, S. T. 1997, ApJ, 486, L23+
- Mathis, J. S., Mezger, P. G., & Panagia, N. 1983, A&A, 128, 212
- Miville-Deschênes, M.-A. & Lagache, G. 2005, ApJS, 157, 302
- Miville-Deschênes, M.-A., Ysard, N., Lavabre, A., et al. 2008, A&A, 490, 1093
- Parravano, A., Hollenbach, D. J., & McKee, C. F. 2003, ApJ, 584, 797
- Pech, C., Joblin, C., & Boissel, P. 2002, A&A, 388, 639
- Schlegel, D. J., Finkbeiner, D. P., & Davis, M. 1998, ApJ, 500, 525
- Sellgren, K., Allamandola, L. J., Bregman, J. D., Werner, M. W., & Wooden, D. H. 1985, ApJ, 299, 416
- Verstraete, L., Pech, C., Moutou, C., et al. 2001, A&A, 372, 981

³ The improvement in the correlations is significant to a confidence level greater than 99.7% for the 27 regions.

⁴ The correlation is also poor with the 60 $\mu\text{m} / G_0$ and for 3 of them with 25 $\mu\text{m} / G_0$ ($P = 0.18$ and $P = 0.7$ for the field in Fig. 3, respectively).